Large reversible magnetocaloric effect and magnetoresistance by improving crystallographic compatibility condition in Ni(Co)-Mn-Ti all-*d*-metal Heusler alloys

Saheli Samanta ●,* Sudipta Chatterjee ●, Subrata Ghosh ●, and Kalyan Mandal ●†

Magnetism Laboratory, Department of Condensed Matter Physics and Material Sciences, S. N. Bose National Centre for Basic Sciences,
JD Block, Sector III, Salt Lake, Kolkata 700106, India

Recently, all-*d*-metal Ni(Co)-Mn-Ti Heusler systems have become the research hotspot due to their magnetoresponsive properties associated with a tunable first-order magnetostructural transformation (MST) and excellent mechanical stability for potential applications. However, the presence of large thermal hysteresis acts as an obstacle to the cyclic operation of this novel material. In this present paper, we investigate a large reversible magnetocaloric effect (MCE) and magnetoresistance (MR) in $Ni_{37-x}Co_{13+x}Mn_{34.5}Ti_{15.5}$ all-*d*-metal Heusler alloys that undergo a first-order MST accompanied by a large magnetization change between ferromagnetic austenite and antiferromagnetic martensite phases. Tuning the small at.% of Co doping in $Ni_{37-x}Co_{13+x}Mn_{34.5}Ti_{15.5}$ systems, we achieved an optimum composition with $x = 1$ where low thermal hysteresis of ~4.7 K, a narrow transformation interval of ~11.2 K, and improved sensitivity of transformation temperature ~2.8 K/T is observed. In addition, the origin of small hysteresis is studied based on geometric compatibility between cubic austenite and monoclinic martensite phases, calculated from the powder x-ray diffraction data. These optimized parameters lead to a reversible magnetic field-induced inverse martensitic transition under the field cycling, yielding a large reversible magnetic entropy change (ΔS_M) of ~17.78 J kg^{-1} K^{-1} at 277 K in a field change of 5 T. Moreover, a large reversible magnetoresistance (MR) of ~14% out of 32.6% is also obtained under 5-T magnetic field for $x = 1$ sample in all-*d*-metal Heusler alloys. These reversible magnetoresponsive properties are comparable to other Ni-Mn-based Heusler alloys and have not been reported so far in the all-*d*-metal Heusler system. Therefore our present work demonstrates a pathway to design new cyclically stable multifunctional materials in all-*d*-metal Heusler systems for solid-state cooling devices and magnetic recording applications.

I. INTRODUCTION

Caloric materials with first-order magnetostructural transitions (MST) are a key element of solid-state-based cooling applications which is deemed as a substitute of conventional cooling technology owing to its higher energy efficiency and environment friendly nature [1]. Since the discovery of room-temperature (RT) giant magnetocaloric effect (MCE) across MST in $Gd_5(Si_2Ge_2)$ [2]. RT magnetic refrigeration has attracted a lot of attention as a reliable and significant energy conversion technology. Furthermore, several classes of materials displaying coupled MST, such as La(Fe, Si)$_{13}$-based materials [3–5], Mn-Ni (Ge, Si) systems [6], and Ni-Mn-*X* (*X* = Ga, In, Sn, Sb) metamagnetic Heusler alloys [7–10] have also been widely investigated for RT solid-state-based applications.

Among the above mentioned systems, Ni-Mn-X Heusler alloys are extensively investigated due to their multifunctional properties like inverse MCE [11–13], magnetic shape memory effect [14], and magnetoresistance (MR) [15–17]. In general, to induce first-order phase transition, the energy is required to overcome the potential barrier between austenite and martensite phases. This energy leads to the intrinsic irreversibilities in the MCE properties during the subsequent field cycling operations. These irreversible behaviors are originated from friction of interface motion, formation of defects and thereby, results both thermal and magnetic hysteresis. Therefore most attempts have been explored to the reduction of hysteresis through improving the compatibility condition between the austenite and martensite phases [7,18–21], modifying the chemical compositions, physical pressure, annealing conditions, minor loops, and measurement of cyclical way [22–24]. However, in those systems, brittleness nature due to field cycling is a challenging issue towards their use in technological applications.

In this regard, all-*d*-metal Ni–Mn-Ti Heusler alloys were developed with excellent ductility using the concept of *d-d* hybridization between transition metals instead of *p-d* hybridization between main group and transition metal of conventional Heusler alloys [25,26]. In the stchoichiometric form, Ni$_2$MnTi alloy usually displays an antiferromagnetic (AFM) like ordering at low temperature ~120 K in the austenite phase, originating from Mn(B)-Mn(D) interaction. Further studies indicated the conversion of AFM interaction into a strong ferromagnetic (FM) Mn(B)-Co/Fe(A,C)-Mn(D) exchange exchange interaction due to the partial Co/Fe

*saheli.trc@bose.res.in
†kalyan@bose.res.in

substitution in Ni site. Hence, MST occurs from a high-temperature strong FM cubic B2-type austenite (spatial group $Pm\bar{3}m$) to a low temperature weak-magnetic monoclinic (spatial group $P2/m$) or tetragonal (spatial group $I4/mmm$) martensite phases [25]. These systems have received enormous interest due to their magnetofunctionalities caused by magnetic field-induced inverse martensitic transition (IMT). For instance, large magnetic entropy change (ΔS_M) of 38 J kg^{-1} K^{-1} driven by a relatively low magnetic field of 2 T across the MST of Ni$_{37}$Co$_{13}$Mn$_{34}$Ti$_{16}$ alloy is reported [27]. Recently, we reported a giant conventional exchange bias field of 3.68 kOe in Ni$_{40}$(FeCo)$_4$Mn$_{36}$Ti$_{20}$ all-d-metal Heusler alloy [28]. In addition, a colossal elastocaloric effect with an large reversable adiabatic temperature change (ΔT_{ad}) up to 31.5 K is achieved in (Ni$_{50}$Mn$_{31.5}$Ti$_{18.5}$)$_{99.8}$B$_{0.2}$ bulk polycrystalline system [29]. Subsequently, a giant barocaloric effect with a large ΔS of 74 J kg^{-1} K^{-1} in the same system is also obtained [30]. Therefore, from the above experimental point of view, the attainable of reversible MCE during subsequent field cycling has not yet been addressed in this particular system, which is important for the technological applications.

From the Clausius Clapeyron (CC) relation, the minimum field required to achieve a complete reversible field-induced IMT and corresponding MCE is

$$\Delta(\mu_0 H)_{min} = (\Delta T_{hys} + \Delta T_{int})/(\Delta M/\Delta S_{tr}), \quad (1)$$

where ΔM is the magnetization change between austenite and martensite phase, ΔT_{hys} is the thermal hysteresis, ΔT_{int}, the transformation interval, and ΔS_{tr} is the transformation entropy change across the transition. Based on the above Eq. (1), the reversibility of field-induced functional properties would be achieved for the smaller ΔT_{hys}, ΔS_{tr}, and narrower ΔT_{int} in Ni(Co)-Mn-Ti all-d-metal systems. Furthermore, $\Delta M/\Delta S_{tr}$ is closely related to the distance between Curie and inverse MT temperature, i.e., ($T_C - T_A$) [31–33]. Hence, it is feasible to modulate $\Delta M/\Delta S_{tr}$ through the tailoring of ($T_C - T_A$) in order to improve the reversible magnetoresponsive properties in IMT under subsequent field cycling in all-d-metal Ni(Co)-Mn-Ti systems.

In the present study, we aim to improve the reversibility of magnetoresponsive properties associated with the IMT in Ni$_{37-x}$Co$_{13+x}$Mn$_{34.5}$Ti$_{15.5}$ all-d-metal Heusler systems. Motivating by the work of Taubel *et al.* [27], our starting material is Ni$_{37}$Co$_{13}$Mn$_{34.5}$Ti$_{15.5}$ which exhibits smaller ΔT_{hys} (5.5 K) and ΔT_{int} (11.7 K), while the presence of large ΔS_{tr} (∼30 J kg^{-1} K^{-1}) and weak sensitivity $dT_M/d\mu_0$H (∼−1.6 K/T) hinders them in technological application. Thus we substituted a small amount of Co in Ni$_{37}$Co$_{13}$Mn$_{34.5}$Ti$_{15.5}$, aiming to improve the reversible properties associated with the magnetostructural transformation. To illustrate the origin of the reversible properties, we used powder x-ray diffraction experiment in order to analyze geometrical compatibility condition which is calculated using the lattice parameters between austenite and martensite phase [21,34,35]. We suggest from experimental results that the obtained geometrical compatibility conditions of martensite and austenite phases could be the basis of lower hysteresis and reversible magnetoresponsive properties in Ni(Co)-Mn-Ti all-d-metal-Heusler systems.

II. EXPERIMENTAL DETAILS

Ni$_{37-x}$Co$_{13+x}$Mn$_{34.5}$Ti$_{15.5}$ ($x = 0$, 1, and 2) polycrystalline samples were prepared by arc melting technique under a 4 N purity argon atmosphere using high purity constituent elements from Sigma Aldrich. The samples were re-melted five to six times on each side to ensure homogenization. The melted ingots were wrapped with a tantalum foil and sealed in a quartz tube under a high vacuum and annealed at 1323 K. Past 4 days of heat treatment, samples were quenched into ice water. The actual compositions of the studied samples were verified by energy dispersive x rays (EDX). The temperature-dependent of x-ray diffraction (XRD) patterns of the sample in powder form was investigated using SmartLab9kW, Rigaku with Cu-K_α radiation. Magnetic measurements were performed in a vibrating sample magnetometer (VSM) using physical property measurement system (PPMS, Quantum design). Differential scanning calorimetry (DSC, TA Instrument, Q2000) was performed to measure the heat flow curve of the sample with a constant heating/cooling rate of 10 K/min. The specific heat capacity (C_P) was measured by modulated-DSC technique. The transport measurements were performed in the PPMS (Quantum Design, USA) using the ac-transport option. For both the resistivity and MR measurements, the electrical contacts were made in the standard four-probe configuration using conducting silver epoxy and copper wires.

III. RESULTS AND DISCUSSIONS

A. Composition optimization by magnetic properties analysis

DSC heat flow measurement is carried out during the heating and cooling sequence at a ramp rate of 10 K/min for all the samples, as exhibited in Fig. 1(a). All samples exhibit endothermic and exothermic peaks, associated with IMT and MT, respectively. The presence of thermal hysteresis (ΔT_{hys}) between endothermic and exothermic peaks confirms the first-order phase transition. The characteristic transition temperatures of the first-order MST namely, austenite start (A_s), austenite finish (A_f), martensite start (M_s), martensite finish (M_f) determined by the tangent method from the DSC curves and corresponding austenite to martensite transition [$T_M = (M_s + M_f)/2$] and the martensite to austenite phase transition [$T_A = (A_s + A_f)/2$], and ($\Delta T_{hys} = T_A - T_M$) of all the samples are tabulated in Table I. Notice that the Co doping in Ni site transformation temperatures decrease considerably which is in agreement with the decrease in e/a ratio of Co with respect to that Ni [36]. Further, due to the interaction between structural and magnetic contributions to the total transformation entropy change (ΔS_{tr}), ΔS_{tr} across the first-order structural transition during heating is measured following the equation:

$$\Delta S_{tr} = \int_{T_i}^{T_f} \frac{dQ}{dT} \left(\frac{dT}{dt}\right)^{-1} \frac{1}{T} dT, \quad (2)$$

where dQ/dT is the heat flow changes of the sample. T_i and T_f are the starting and finishing temperatures of the first-order phase transition, respectively. The obtained ΔS_{tr} for all the samples is gathered in Table I.

Figures 1(b)–1(d) represents the temperature-dependent magnetization data for all the samples. On decreasing the
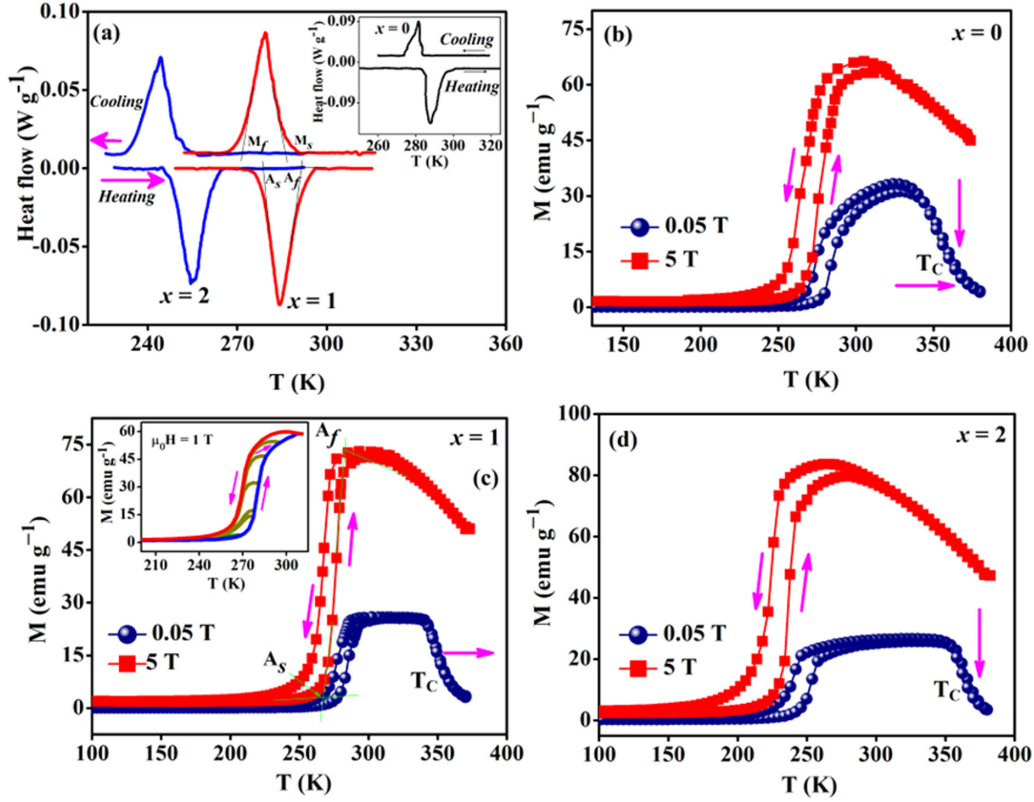
FIG. 1. (a) DSC heat-flow measurement for all the alloys. Isofield-magnetization $M(T)$ curve of $Ni_{37-x}Co_{13+x}Mn_{34.5}Ti_{15.5}$ for (b) $x = 0$, (c) 1, and (d) 2 samples at magnetic field of 0.05 and 5 T. (Inset shows minor hysteresis loop of $x = 1$ sample during heating.)

temperature, all samples exhibit a first-order MST from FM austenite to weak magnetic martensite below the Curie temperature T_C. With increasing magnetic field, the T_M and T_A move towards lower temperature, in agreement with the magnetic field stabilizing the FM cubic austenite phase with high magnetization. A shift in T_M of ~9, ~12, and ~16 K towards low temperature and the corresponding shift of T_A of ~8, ~10, and ~15 K is observed for $x = 0$, 1, and 2 samples, respectively towards lower temperature due to the change in magnetic field change from 0.05 to 5T. Hence, the sensitivity of transition temperatures to the magnetic field obtained from linear fitting of T_M versus field (see Fig. S1 of Ref. [37]) are mentioned in Table I. This value is rather weak compared to the Ni-Mn-In alloys [34,35,38] yet higher than the Ni-Mn-Ti all-d-metal Heusler alloys [39], and Mn-Ni-Ge-based system [40]. On the basis of the CC equation $dT_M/d\mu_0H = \Delta M/\Delta S_{tr}$, the sensitivity not only depends on the magnetization change but also ΔS_{tr} [13] and corresponding to $(T_C - T_A)$, i.e., larger the $(T_C - T_A)$, weaker the ΔS_{tr} at the

transition, which leads to a larger $dT_M/d\mu_0H$ (and thus reversible MCE) [31–33]. In view of this, Co substitution for Ni site in $Ni_{37-x}Co_{13+x}Mn_{34.5}Ti_{15.5}$ all-d-metal Heusler alloys, increases the value of $(T_C - T_A)$ and decreases ΔS_{tr}. Clearly, $x = 1$ possess relatively smaller ΔT_{hys}, ΔT_{int}, and lower critical field $\Delta(\mu_0H)_{min}$ of about 4.5 T. On the contrary, the $x = 2$ shows much larger $\Delta T_{hys} + \Delta T_{int}$ as well as $\Delta(\mu_0H)_{min}$, which is about 5.7 T and hence it is hard to achieve a complete phase transformation under 5 T, hence resulting in a small magnetoresponsive properties. Therefore the alloy with $x = 1$ is more favorable for the further reversible magnetoresponsive properties studies.

It is reported that the reversible field-induced IMT in presence of certain magnetic field μ_0H is occurred when the shift of $M(T)$ curve is higher than the thermal hysteresis [41]. Consequently, the reversible MCE across the field-driven IMT is expected over a temperature window between A_S under μ_0H and M_S under zero field [42]. Therefore the reversible MCE can be obtained in a large temperature window from

TABLE I. Transition temperatures (K) and transformation entropy change obtained from DSC curves of $Ni_{37-x}Co_{13+x}Mn_{34.5}Ti_{15.5}$ all-d-metal Heusler alloys.

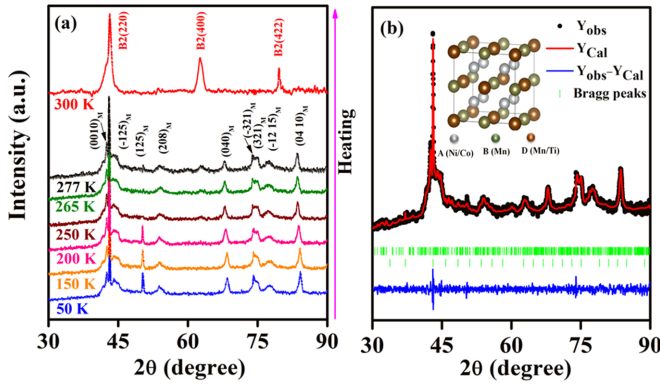| Alloys	M_s (K)	M_f (K)	A_s (K)	A_f (K)	T_M (K)	T_A (K)	ΔT_{int} (K)	ΔT_{hys} (K)	ΔS_{tr} (J kg K^{-1})
$x = 0$	283.2	274.3	286.1	292.3	278.6	289.2	8.9	10.6	22.5
$x = 1$	286.1	272.9	278.5	290.1	280.5	285.2	11.2	4.7	19.89
$x = 2$	250.3	235.3	244.6	261.1	242.8	252.9	15	10.1	18.89

FIG. 2. (a) Temperature-dependent XRD pattern at various temperatures for $Ni_{36}Co_{14}Mn_{34.5}Ti_{15.5}$ alloys ($x = 1$ sample) recorded during heating. (Cubic and monoclinic phase are denoted as "B2" and "5M," respectively.) (b) Rietveld profile refinement of XRD pattern of the same sample at 277 K. Inset shows the cubic crystal structure and individual atomic site occupation.

267.5 K (A_S) at 5 T to 286.1 K (M_S) from DSC for $x = 1$ sample, as shown in the Fig. 1(c).

B. Geometric compatibility condition from structural analysis

In magnetic shape memory alloys (SMAs), the presence of small thermal hysteresis is strongly related to the austenite and martensite phases and their interfaces (known as habit plane) [20,21,43,44]. Recently, it has been widely reported that not only small hysteresis yet narrow transformation interval is resulted by improving the geometrical compatibility condition between both phases and established certain condition for it [18–20]. Mathematically, the condition, $\lambda_2 = 1$, where $\lambda_1 \geqslant \lambda_2 \geqslant \lambda_3$ are the order eigenvalues of the transformation stretch matrix U, represents the existence of an invariant plane between both phases. The U is defined as a homogeneous 3×3 deformation matrix. In the case of complete reversible MCE, the λ_2 of U is 1. To determine U for our system, the temperature dependent powder XRD experiment is carried out for $x = 1$ sample and depicted in Fig. 2(a). Noticeably, the sample experiences the transition from a martensitic phase with a five-modulated (5M) monoclinic structure to a cubic austenite phase during heating and the crystal orientation relation between the 5M martensite and B2 austenite phases; $\sqrt{2}a_M = a_c$; $b_M = a_c$; $\sqrt{2}c_M/5 = a_c$, and $2V_M = V_A$ [45]. A small fraction of martensite at 300 K can be appeared due to the residual stress generated during the grinding of the ingot into powder [46]. From the Fig. 2(b), the refined lattice parameters, at 277 K where both phases coexist, are $a_M = 4.342$ Å, $b_M = 5.5136$ Å, $c_M = 21.0359$ Å, and $\beta_M = 90.95$ for martensite and $a_c = 5.921$ Å for the austenite phase. Theoretically, in the cubic to monoclinic transformation, there are 12 corresponding variants for monoclinic structure of martensite phase, where these variants have the same eigenvalue, eigen energy, and volume changes [35]. The transformation stretch matrix of one of the corresponding variants of martensite

phase is given by

$$U = \begin{pmatrix} \tau & \sigma & 0 \\ \sigma & \rho & 0 \\ 0 & 0 & \delta \end{pmatrix},$$

where the deformations are given by

$$\tau = \frac{\alpha^2 + \gamma^2 + 2\alpha\gamma(\sin\beta - \cos\beta)}{2\sqrt{\alpha^2 + \gamma^2 + 2\alpha\gamma\sin\beta}}, \tag{3}$$

$$\rho = \frac{\alpha^2 + \gamma^2 + 2\alpha\gamma(\sin\beta + \cos\beta)}{2\sqrt{\alpha^2 + \gamma^2 + 2\alpha\gamma\sin\beta}}, \tag{4}$$

$$\sigma = \frac{\alpha^2 - \gamma^2}{2\sqrt{\alpha^2 + \gamma^2 + 2\alpha\gamma\sin\beta}}, \tag{5}$$

$$\delta = \frac{b_M}{a_c} \tag{6}$$

with $\alpha = \sqrt{2}a_M/a_c$ and $\gamma = \sqrt{2}c_M/Na_c$ [47,48], a_c is the lattice parameter of a cubic austenite phase and a_M, b_M, c_M, and the angle β denote the lattice parameters of a monoclinic unit cell. Now the transformation matrix of the $x = 1$ sample is

$$U = \begin{pmatrix} 1.0293 & 0.0161 & 0 \\ 0.0161 & 1.0124 & 0 \\ 0 & 0 & 0.9311 \end{pmatrix}.$$

The eigenvalues of the above matrix for $x = 1$ sample are 1.0353, 1.0065, and 0.9378. It is shown that the λ_2 is very closed to 1 and hence, $|1 - \lambda_2| = 0.0065$ with the deviation of 0.65% from the unity indicates that the geometric compatibility between the two phases is significantly improved [19,47–49]. As a result, a small hysteresis alongwith good reversibility is obtained in Ni-Co-Mn-Ti all-d-metal Heusler alloys. We demonstrated that the reversibility of magnetocaloric materials is significantly enhanced by following minor hysteresis loop for $x = 1$ sample (details are shown in Fig. S2 of Ref. [37]). It is understood by the fact that less energy for nucleation is required in the minor loop of martensitic transformation. Therefore a large fraction 52% of martensite at the IMT temperature upon heating mode is involved to contribute in reducing the hysteresis [50–52]. Thus we can expect that through the minor loop process, a large reversible magnetocaloric effect can be achieved in $Ni_{36}Co_{14}Mn_{34.5}Ti_{15.5}$ all-d-metal Heusler alloy.

C. Reversible magnetocaloric performances

To achieve higher efficiencies in magnetic cooling refrigeration, the reproducibility of the first-order magnetic-field-induced transformation upon magnetic field cycling is crucial. For that, isothermal magnetization $M(\mu_0 H)$ curves are measured during cyclic magnetic field sweeping in the temperature range between 268 to 283 K with an interval of 3 K and the results are depicted in Fig. 3(a). During the first field cycle, the sample is first cooled down to 150 K to ensure the fully martensitic phase from 320 K and then heated back to the respective temperatures where the $M(\mu_0 H)$ data are taken [53,54]. In the second field cycle, $M(\mu_0 H)$ data at the same temperature are measured just after the first cycle of field sweeping. Noticeably, the sample exhibits a strong metamagnetic behavior between 268 and 283 K, indicating
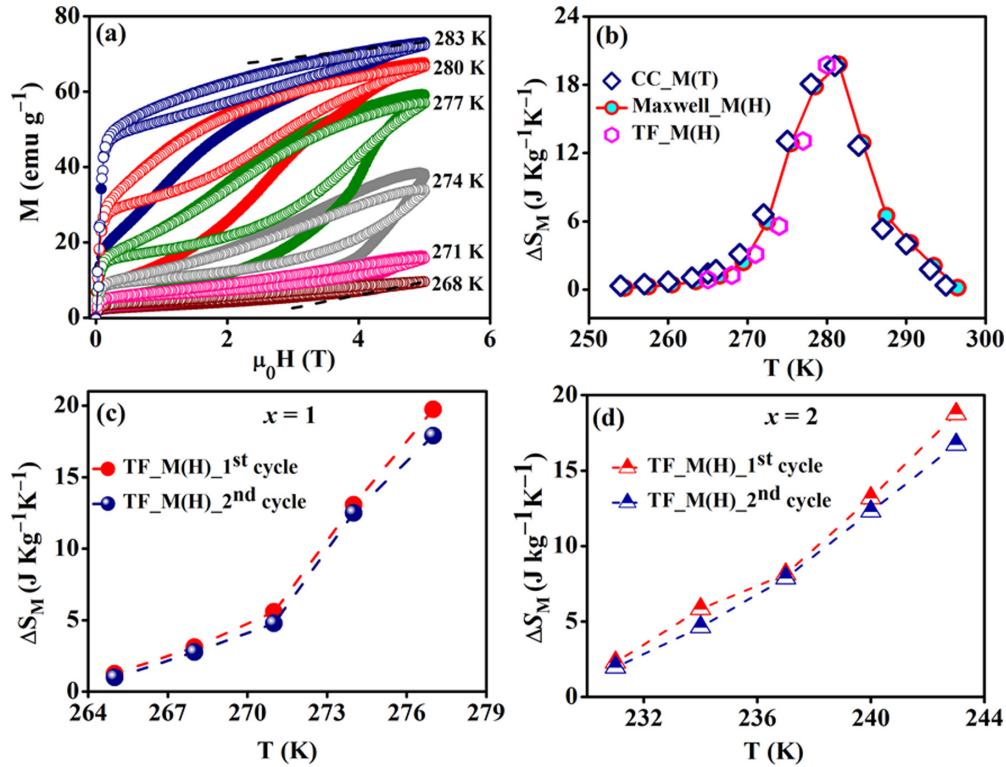
FIG. 3. (a) Isothermal $M - \mu_0 H$ hysteresis measured during the first (solid circle) and second (hollow circle) cycles of field sweeping at 268, 271, 274, 277, 280, and 283 K during heating for $x = 1$ sample. (b) Comparison of ΔS_M vs T during the first field cycle at 5 T determined with the various methods through the Maxwell relation [Maxwell $M(H)$], Clausius Clapeyron relation [CC_$M(T)$ and transformation fraction method (TF_$M(-H)$], and (c) ΔS_M vs T by TF_$M(H)$] during the first and second field cycles of the $x = 1$ sample (d) of $x = 2$ sample, where the second cycle ΔS_M is reversible.

magnetic field-induced IMT from weak magnetic martensite to FM austenite. At the temperature ($\sim$268 K) close to A_S, the $M(\mu_0 H)$ curves of both cycles match with each other, suggesting the MST is completely reversible. However, from the temperature $\sim$271 to 280 K, the low field magnetization in $M(\mu_0 H)$ curves of the second cycle is higher than the first one. It is also noted that the $M(\mu_0 H)$ curves recorded during the third and following field cycles coincide with the second field cycle. This yields a good reversibility of IMT in the system after the first field cycle. At 283 K, no martensite phase is recovered after the first cycle, exhibiting that IMT does not occur after 283 K, upon the field cycling [41,55].

Now we quantitatively explain the above results based on the reversible effect in the Ni-(Co)-Mn-Ti all-d-metal system. When the field of 5 T is applied above A_S, for instance, from 268 to 280 K, the magnetic field prefers to stabilize the FM state, the field-induced IMT is occurred along with large magnetic hysteresis. Upon descending the magnetic field from 5 T, as a result of ΔT_{hys}, the induced austenite cannot fully transform back to martensite and therefore, residual austenite is conserved. So, this residual austenite causes higher magnetization of the second cycle due to its FM nature. During the second and all subsequent field cycling with small ΔT_{hys}, the martensite that is reverted during first descending field can participate reversibly to transform back and forth between martensite and austenite. Therefore this portion of the sample could yield a reversible and reproducible magnetocaloric effect.

Isothermal magnetic entropy change (ΔS_M) is an important parameter to quantify MCE response of the investigated alloys which can be computed across T_A, using Maxwell relation [1],

$$\Delta S_M(T, \Delta H) = \mu_0 \int_0^H \left(\frac{\partial M(H, T)}{\partial T} \right)_H dH \qquad (7)$$

where μ_0, M, H, and T are the permeability of free space, magnetization, applied magnetic field, and instantaneous temperature, respectively. The maximum value of $\Delta S_M \sim$19.78 J kg^{-1} K^{-1} at 281.5 K is obtained for $x = 1$ under 5 T, shown in Fig. 3(b) which is in good agreement with ΔS_{tr}, determined from the DSC curve (in Table I).

For a more comprehensive and reliable analysis, the ΔS_M is also deduced using different methods. Clausius-Clapeyron equation using transformation fraction method is appropriate for the first-order MST and is employed here to deduce ΔS_M values from isofield M-T measurements for the different field changes [56].

$$\Delta S_M = -\Delta f \Delta M \left(\frac{\Delta T_t}{\Delta \mu_0 H} \right)^{-1}, \qquad (8)$$

where Δf is the change of phase fraction of austenite induced by the change of magnetic field that can be defined as $\Delta f(T, \mu_0 \Delta H) = f(T, \mu_0 H_f) - f(T, \mu_0 H_i)$. $\mu_0 H_i$, and $\mu_0 H_f$ are the initial and final applied magnetic field, respectively. The phase volume fraction of austenite can be assumed as proportional to the total magnetization and can be

TABLE II. Comparison of reversible magnetic entropy change (ΔS_M) at 5 T and their respective transition temperatures (T^{peak}) of all-d-$Ni_{37-x}Co_{13+x}Mn_{34.5}Ti_{15.5}$ Heusler alloys, and other related promising systems.

Materials	$|\Delta S_M^{\mathrm{peak}}|$ $(\mathrm{JKg^{-1}K^{-1}})$	T^{peak} (K)	References
Gd	10.2	294	[59]
$Gd_5(Si_2Ge_2)$	18.5	278	[2]
$Ni_{49.8}Co_{1.2}Mn_{33.5}In_{15.5}$	14.6	235	[60]
$Ni_{49}Co_3Mn_{34}In_{14}$	16.5	268	[38]
$Ni_{50.7}V_{0.3}Mn_{33.4}In_{15.6}$	18.9	276	[61]
$Ni_{41.5}Co_{9.2}Mn_{32}Ga_{14}In_{3.3}$	11	-	[62]
$Ni_{41}Ti_1Co_9Mn_{39}Sn_{10}$	18.7	287	[9]
$Ni_{1.9}Pt_{0.1}Mn_{1.4}In_{0.6}$	12	262	[47]
$Mn_{1.87}Cr_{0.13}Sb_{0.95}Ga_{0.05}$	5.2	280	[63]
$Ni_{37-x}Co_{13+x}Mn_{34.5}Ti_{15.5}$ $x=1$	17.8	277	Present work

estimated as [56]

$$f(T) = \frac{M(T) - M_M(T)}{M_A(T) - M_M(T)}, \qquad (9)$$

where $M_M(T)$ and $M_A(T)$ represent the magnetization of the low-temperature and high-temperature phases, respectively. The maximum ΔS_M for the field changes from $H_i \sim 50$ mT to $H_f \sim 5$ T is 19.66 J kg^{-1} K^{-1}, plotted in Fig. 3(b). The result obtained from both Maxwell relation and CC equation confirms that our ΔS_M values are reliable [57].

Furthermore, from the viewpoint of practical application, to achieve reversible and reproducible MCE, the transformation fraction method based on $M(\mu_0 H)$ curve is a feasible and reliable procedure [9]. The phase fraction of austenite is determined from the $M(\mu_0 H)$ curve of both cycles at the respective temperatures using the following equation:

$$f(T) = \frac{M(H) - M_M(H)}{M_A(H) - M_M(H)}, \qquad (10)$$

where $M_M(\mathrm{H})$ and $M_A(\mathrm{H})$ represent the magnetization of the martensite and austenite phase which can be deduced by the extrapolating of $M(\mu_0 H)$ curve at 250 and 300 K of pure martensite and austenite phases, respectively [58]. Figure 3(b) renders the ΔS_M value based on the various methods as a function of temperature during the first field cycle for $x = 1$ sample under the field changes of 5 T. Evidently, the value of ΔS_M estimated from TF_$M(\mu_0 H)$ is almost consistent with the CC_$M(T)$ and Maxwell equation. As mentioned earlier, the field-induced transformation is reversible during second and subsequent field cycles in the temperature range from 265 to 280 K and in Fig. 3(c) we compared ΔS_M using TF_$M(\mu_0 H)$ method for first and second cycles (details are shown in Fig. S3 of Ref. [37]). It is seen that ΔS_M value of second cycle is quite close to that of the first one, indicating good reversibility of the MCE. Hence, a large reversible ΔS_M of 17.78 J kg^{-1} K^{-1} over a broad temperature window $\sim$12 K is achieved upon 5 T, since a large fraction of IMT is involved to contribute in the MCE. For comparison, similar measurements are carried out for $x = 2$ sample and illustrated in Fig. S4 in Ref. [37]). Here, the ΔS_M value at 243 K of $x = 2$ sample obtained from TF_$M(\mu_0 H)$ method for first and second cycles are 18.76 and 16.72 J kg^{-1} K^{-1}, respectively, depicted in

Fig. 3(d). The ΔS_M value of second field cycles are about 11% smaller than the first cycle because the relatively large residual austenite formed during first field ascending does not take part in the transformation during subsequent field cycles. Therefore $x = 1$ sample produces large reversible entropy change which represent nearly 90% of total magnetic entropy change obtained at the first field cycle. The magnitude of reversible ΔS_M is comparable with the highest value reported in the other related promising systems (shown in Table II) which is indeed beneficial in potential application.

Adiabatic temperature change (ΔT_{ad}) is another important parameter to quantify the MCE. It is reported that the reversible ΔT_{ad} is roughly estimated using the measuring temperature-dependent specific heat capacity (C_p) following the equation:

$$\Delta T_{\mathrm{ad}} = -\frac{T}{C_p} \times \Delta S_M. \qquad (11)$$

C_p has been recorded in zero field condition using modulated DSC technique as shown as a function of temperature in Fig. 4(a). The reversible ΔT_{ad}, is deduced from the reversible ΔS_M data in Fig. 3(c) and the C_p values presented in Fig. 4(a), which is ploted as a function of temperature in Fig. 4(b). A maximum reversible $\Delta T_{\mathrm{ad}} \sim$6.7 K is obtained in $Ni_{37-x}Co_{13+x}Mn_{34.5}Ti_{15.5}$ all-d-metal alloys and this magnitude is comparable to other Ni-Mn-X Heusler alloys [9,38,40,55,64].

It is well known that the cyclic behavior of phase transformation plays a significant role on the mechanical stability of the MCE materials. We plotted in Fig. 5(a) the thermal cycling behavior for the alloy with $x = 1$ measured by DSC and their respective characteristic temperatures vs. cycle are presented in Fig. 5(b). Clearly, the peak positions remain almost unchanged and no significant shift of the characteristic temperatures is observed over 35 thermal cycles. Therefore this observation demonstrates that the phase transition posses a good reversibility and stability in our system.

D. Magnetoresistance

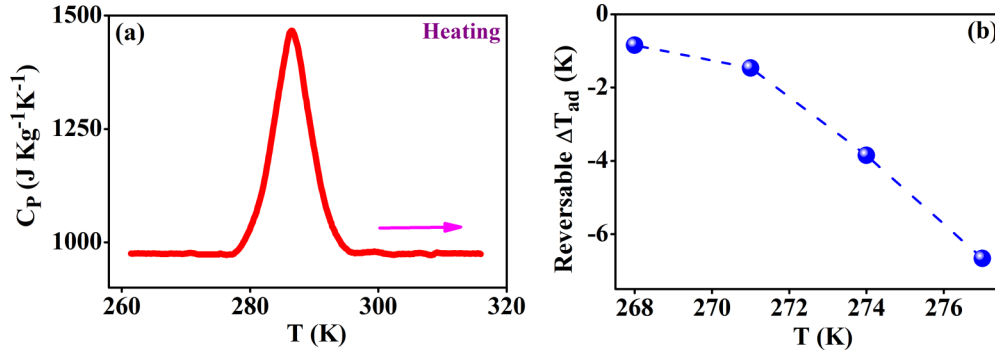The structural transformations in the Heusler alloys are realized by the band John-Teller effect. They are accompanied

FIG. 4. (a) Specific heat capacity (C_P) as a function of temperature under zero field for the $Ni_{36}Co_{14}Mn_{34.5}Ti_{15.5}$ alloy recorded during heating mode. (b) Reversible ΔT_{ad} vs $T(K)$ under 5 T obtained from Eq. (10).

by the change of fundamental ordering of spins and consequently the crystal and magnetic structure which causes to a significant change in the electrical resistance. To investigate the magnetoresistive properties and their reversibility, we measured the temperature and magnetic field dependent electrical resistivity of $x = 1$ sample and are shown in Fig. 6. It is seen [in Fig. 6(a)] that on cooling, $\rho(T)$ exhibits an abrupt increase around the MST. This is caused by the change in the electronic density of state in the vicinity of Fermi level due to the lattice distortion of the phase transformation [65]. On the application of a magnetic field of 5 T, A_S is reduced by $\sim$11 K with the reduction rate of 2.2 K/T. Hence, there exists a certain temperature gap between the resistivity at 259.6 K (A_S) upon 5 T to that at 277.3 K (M_S) under 0 T, which indicates that a partial reversible behavior of MR is expected in the above-mentioned temperature range.

The inset of Fig. 6(a) exhibits the temperature dependence of MR under a magnetic field change of $\mu_0 H$ during heating is obtained from the following equation:

$$MR = \left[\frac{R(\mu_0 H) - R(0)}{R(0)} \right] \times 100\%, \qquad (12)$$

where $R(\mu_0 H)$ and $R(0)$ stand for the electrical resistance under $\mu_0 H$ and zero field. A maximum MR value of -32.6% is observed across the IMT under the field of 5 T which is comparable to other Ni-Mn-based Heusler alloys [66–68]. This large negative MR is developed as the electrical resistance

in the austenite state is much lower than that the martensite phase. On applying the magnetic field, a field-induced inverse transformation from weak magnetic martensitic state to FM austenite state is developed, leading to the negative MR.

To get a further insight of reversible MR, the isothermal resistivity versus field is studied upon subsequent field cycling and the corresponding field dependent MR is depicted Figs. 6(c) and Fig. 6(e), respectively. At 300 K, the sample is in the fully austenite state and no significant change in MR is observed when a field is applied. One can observe that with increasing temperature in the reverse IMT region, for example, at 265, 270, and 277 K, the critical field decreases with increasing field because reverse IMT is induced by the field from the martensite to austenite state. Notably, the peak value of MR increases with the measured temperature because of the enhancement of the volume fraction of martensite by the application of magnetic field of 5 T. After that, upon removal of the field, the MR does not reverse entirely into the initial state. As a consequence, a reduced reversible MR of about 14% is obtained at 277 K for the second and subsequent field cyclic measurements. Compared to the reversible MR of sample $x = 1$, the analogous $\rho(T)$ and $\rho - \mu_0 H$ measurements are illustrated in Figs. 6(b), 6(d) and 6(f) for $x = 2$ sample. An applied of magnetic field 5T resulted in a decrease of A_s by 17.1 K with the reduction rate of 3.4 K/T, which is well consistent with the result from M(T) curve. Hence, the partial reversible field-induced IMT may occurs between 232.8 K
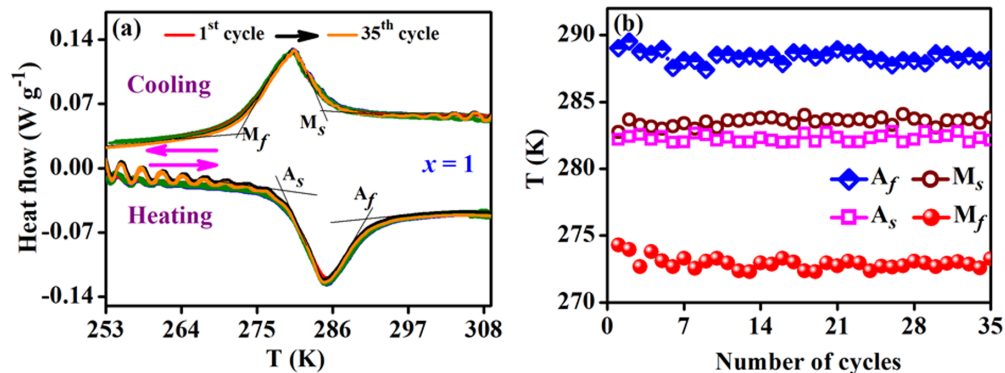

FIG. 5. (a) DSC heat-flow curves during heating and cooling cycles (b) The characteristic transformation temperatures under 35 thermal cycles of $x = 1$ sample.
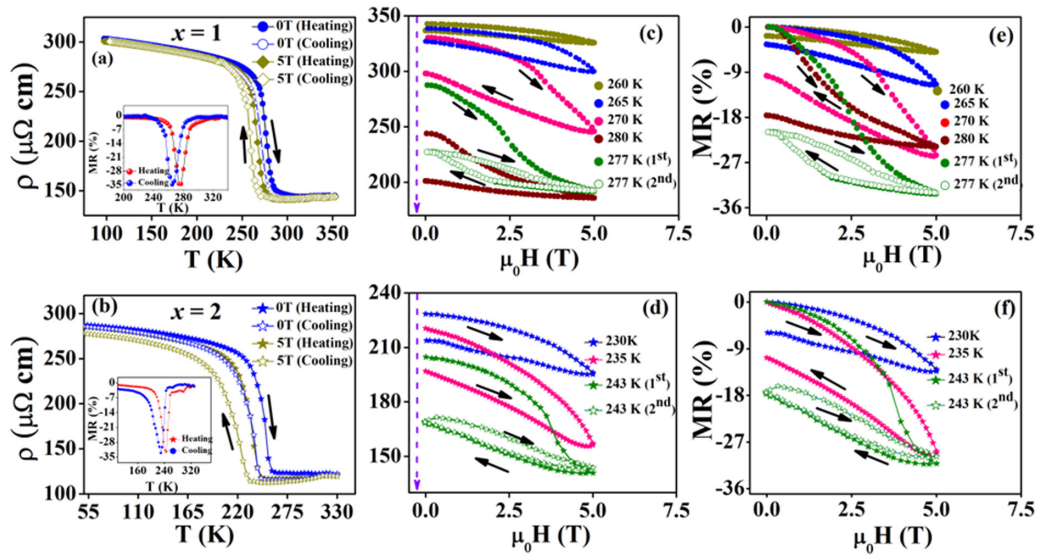
FIG. 6. [(a) and (b)] Temperature-dependent electrical resistivity ($\rho - T$) curves of $x = 1$ and $x = 2$ samples upon heating and cooling with 0 and 5 T. Inset shows the corresponding temperature dependence of MR during heating and cooling cycles. [(c) and (d)] Field-dependent resistivity ($\rho - \mu_0 H$) at various temperatures upon heating mode across the transition of $x = 1$ and $x = 2$ samples. The green hollow circle represents the second cycle ($\rho - \mu_0 H$) at 277 K after the first cycle of magnetic field. [(e) and (f)] The corresponding field dependence of MR of those samples, respectively in the inverse martensitic region.

(A_s) upon 5 T and 250.3 K (M_s) under 0 T. Figures 6(d) and 6(f) show the field-dependent resistivity and corresponding MR in the reverse IMT region. It is observed from Fig. 6(d) that at 230 and 235 K, the resistivity decreases with increasing temperature and very weak field-induced transition occurs with increasing the magnetic field. The same phenomena is observed in the M-$\mu_0 H$ curve (in Fig. S4 in Ref. [37]). So, for the evaluation of reversible MR, second cycle of $\rho - \mu_0 H$ curve are record with the first one at 243 K. It is seen that at 243 K, large fraction of residual austenite of the first field descending cycle persists for subsequent field cycling [69]. As a consequence of that, a relatively small reversible MR of about 13.1% during the second cycle of the total MR $\sim$31.2% during first cycle at 243 K is obtained. Therefore relatively large temperature window of the reversible MR and near room temperature working temperature highly favors the sample $x = 1$ as magnetic actuator for technological application.

IV. CONCLUSIONS

In summary, the reversibility of both the MCE and MR has been experimentally investigated using different measurement protocols. The reversibility of magnetoresponsive properties depend upon the two competing factors, field-induced shift of the transformation temperatures and the width of the hysteresis. Thus systematically tuning with the small at.% of Co addition in Ni site, a small ΔT_{hys}, narrow ΔT_{int} and improved sensitivity of $\sim$2.8 K/T is observed in the $x = 1$ sample.

The origin of the small ($\Delta T_{hys} + \Delta T_{int}$) is related to the middle eigenvalue i.e., $\lambda_2 = 1.0065$ of the transformation stretch matrix U which is closed to one, confirming good geometrical compatibility between two phases in all-d-metal Heusler alloys. In addition, the minor hysteresis loop has been done in order to enhance the reversibility of our system. A large reversible ΔS_M of $\sim$17.78 J kg^{-1} K^{-1} at 277 K over a broad temperature window $\sim$12 K has been deduced in the studied alloy. Moreover, due to partial reversible field-induced inverse MT, a large reversible MR of 14% out of 32.6% is obtained. The present work also demonstrates that narrower hysteresis loop in $x = 1$ sample is more beneficial for reversible multifunctional properties than the larger magnetization difference in $x = 2$ sample. These reversible magnetoresponsive properties are comparable to other Ni-Mn-based Heusler alloys and have not been reported so far in the all-d-metal Heusler system. Therefore these findings illuminate new potential functionalities in Ni(Co)-Mn-Ti all-d-metal Heusler alloys and make them attractive candidates as a cyclically stable caloric material with small hysteresis for magnetic refrigeration and magnetic recording applications.

[1] K. A. GschneidnerJr, V. K. Pecharsky, and A. O. Tsokol, Rep. Prog. Phys. **68**, 1479 (2005).

[2] V. K. Pecharsky and K. A. Gschneidner, Jr., Phys. Rev. Lett. **78**, 4494 (1997).

[3] A. Fujita, S. Fujieda, Y. Hasegawa, and K. Fukamichi, Phys. Rev. B **67**, 104416 (2003).

[4] V. Franco, J. Blázquez, J. Ipus, J. Law, L. Moreno-Ramírez, and A. Conde, Prog. Mater. Sci. **93**, 112 (2018).

[5] O. Gutfleisch, T. Gottschall, M. Fries, D. Benke, I. Radulov, K. P. Skokov, H. Wende, M. Gruner, M. Acet, P. Entel, *et al.*, Philos. Trans. R. Soc. A **374**, 20150308 (2016).

[6] T. Samanta, D. L. Lepkowski, A. U. Saleheen, A. Shankar, J. Prestigiacomo, I. Dubenko, A. Quetz, I. W. H. Oswald, G. T. McCandless, J. Y. Chan, P. W. Adams, D. P. Young, N. Ali, and S. Stadler, Phys. Rev. B **91**, 020401(R) (2015).

[7] A. A. Mendonça, L. Ghivelder, P. L. Bernardo, H. Gu, R. D. James, L. F. Cohen, and A. M. Gomes, Phys. Rev. Mater. **4**, 114403 (2020).

[8] X. He, Y. Zhang, S. Wei, Y. Cao, K. Xu, and Z. Li, J. Phys. D **54**, 165001 (2021).

[9] Y. Qu, D. Cong, X. Sun, Z. Nie, W. Gui, R. Li, Y. Ren, and Y. Wang, Acta Mater. **134**, 236 (2017).

[10] S. J. Kim, W. H. Ryu, H. S. Oh, and E. S. Park, J. Appl. Phys. **123**, 033903 (2018).

[11] T. Krenke, E. Duman, M. Acet, E. F. Wassermann, X. Moya, L. Mañosa, and A. Planes, Nat. Mater. **4**, 450 (2005).

[12] J. Liu, T. Gottschall, K. P. Skokov, J. D. Moore, and O. Gutfleisch, Nat. Mater. **11**, 620 (2012).

[13] R. Kainuma, Y. Imano, W. Ito, Y. Sutou, H. Morito, S. Okamoto, O. Kitakami, K. Oikawa, A. Fujita, T. Kanomata, *et al.*, Nature (London) **439**, 957 (2006).

[14] Z. H. Liu, M. Zhang, Y. T. Cui, Y. Q. Zhou, W. H. Wang, G. H. Wu, X. X. Zhang, and G. Xiao, Appl. Phys. Lett. **82**, 424 (2003).

[15] R. Kainuma, Y. Imano, W. Ito, H. Morito, Y. Sutou, K. Oikawa, A. Fujita, K. Ishida, S. Okamoto, O. Kitakami, and T. Kanomata, Appl. Phys. Lett. **88**, 192513 (2006).

[16] M. Khan, I. Dubenko, S. Stadler, and N. Ali, J. Appl. Phys. **102**, 113914 (2007).

[17] L. Chen, F. X. Hu, J. Wang, L. F. Bao, J. R. Sun, B. G. Shen, J. H. Yin, and L. Q. Pan, Appl. Phys. Lett. **101**, 012401 (2012).

[18] Y. Song, X. Chen, V. Dabade, T. W. Shield, and R. D. James, Nature (London) **502**, 85 (2013).

[19] R. Zarnetta, R. Takahashi, M. L. Young, A. Savan, S. Furuya, S. Thienhaus, B. Maaß, M. Rahim, J. Frenzel, H. Brunken, Y. S. Chu, V. Srivastava, R. D. James, I. Takeuchi, G. Eggeler, and A. Ludwig, Adv. Funct. Mater. **20**, 1917 (2010).

[20] J. Cui, Y. S. Chu, O. O. Famodu, Y. Furuya, J. Hattrick-Simpers, R. D. James, A. Ludwig, S. Thienhaus, M. Wuttig, Z. Zhang, *et al.*, Nat. Mater. **5**, 286 (2006).

[21] L. E. L. Silva, J. C. Patiño, and A. M. Gomes, J. Phys.: Condens. Matter **33**, 235701 (2021).

[22] E. Stern-Taulats, A. Planes, P. Lloveras, M. Barrio, J.-L. Tamarit, S. Pramanick, S. Majumdar, S. Yüce, B. Emre, C. Frontera, and L. Mañosa, Acta Mater. **96**, 324 (2015).

[23] Z. Wei, Y. Shen, Z. Zhang, J. Guo, B. Li, E. Liu, Z. Zhang, and J. Liu, APL Mater. **8**, 051101 (2020).

[24] M. Ghorbani Zavareh, C. Salazar Mejía, A. K. Nayak, Y. Skourski, J. Wosnitza, C. Felser, and M. Nicklas, Appl. Phys. Lett. **106**, 071904 (2015).

[25] Z. Y. Wei, E. K. Liu, J. H. Chen, Y. Li, G. D. Liu, H. Z. Luo, X. K. Xi, H. W. Zhang, W. H. Wang, and G. H. Wu, Appl. Phys. Lett. **107**, 022406 (2015).

[26] Z. Y. Wei, E. K. Liu, Y. Li, X. L. Han, Z. W. Du, H. Z. Luo, G. D. Liu, X. K. Xi, H. W. Zhang, W. H. Wang, and G. H. Wu, Appl. Phys. Lett. **109**, 071904 (2016).

[27] A. Taubel, B. Beckmann, L. Pfeuffer, N. Fortunato, F. Scheibel, S. Ener, T. Gottschall, K. P. Skokov, H. Zhang, and O. Gutfleisch, Acta Mater. **201**, 425 (2020).

[28] S. Samanta, S. Ghosh, and K. Mandal, J. Phys.: Condens. Matter **34**, 105801 (2022).

[29] D. Cong, W. Xiong, A. Planes, Y. Ren, L. Mañosa, P. Cao, Z. Nie, X. Sun, Z. Yang, X. Hong, and Y. Wang, Phys. Rev. Lett. **122**, 255703 (2019).

[30] A. Aznar, A. Gràcia-Condal, A. Planes, P. Lloveras, M. Barrio, J.-L. Tamarit, W. Xiong, D. Cong, C. Popescu, and L. Mañosa, Phys. Rev. Mater. **3**, 044406 (2019).

[31] C. Salazar Mejía, M. Ghorbani Zavareh, A. K. Nayak, Y. Skourski, J. Wosnitza, C. Felser, and M. Nicklas, J. Appl. Phys. **117**, 17E710 (2015).

[32] E. Cesari, D. Salas, and S. Kustov, in *Materials Science Forum* (Trans Tech Publ, 2011), Vol. 684, pp. 49–60

[33] T. Kihara, X. Xu, W. Ito, R. Kainuma, and M. Tokunaga, Phys. Rev. B **90**, 214409 (2014).

[34] C. Salazar-Mejía, P. Devi, S. Singh, C. Felser, and J. Wosnitza, Phys. Rev. Mater. **5**, 104406 (2021).

[35] P. Devi, C. S. Mejía, M. G. Zavareh, K. K. Dubey, P. Kushwaha, Y. Skourski, C. Felser, M. Nicklas, and S. Singh, Phys. Rev. Mater. **3**, 062401(R) (2019).

[36] T. Krenke, M. Acet, E. F. Wassermann, X. Moya, L. Mañosa, and A. Planes, Phys. Rev. B **73**, 174413 (2006).

[37] See Supplemental Material at http://link.aps.org/supplemental/ 10.1103/PhysRevMaterials.6.094411 for extra information about the thermal and magnetic analysis, minor hysteresis loop measurement, and magnetic entropy change for a field change of 5 T.

[38] X. M. Sun, D. Y. Cong, Z. Li, Y. L. Zhang, Z. Chen, Y. Ren, K.-D. Liss, Z. Y. Ma, R. G. Li, Y. H. Qu, Z. Yang, L. Wang, and Y. D. Wang, Phys. Rev. Mater. **3**, 034404 (2019).

[39] Z. Guan, X. Jiang, J. Gu, J. Bai, X. Liang, H. Yan, Y. Zhang, C. Esling, X. Zhao, and L. Zuo, Appl. Phys. Lett. **119**, 051904 (2021).

[40] J. Liu, Y. Gong, Y. You, X. You, B. Huang, X. Miao, G. Xu, F. Xu, and E. Brück, Acta Mater. **174**, 450 (2019).

[41] E. Stern-Taulats, P. O. Castillo-Villa, L. Mañosa, C. Frontera, S. Pramanick, S. Majumdar, and A. Planes, J. Appl. Phys. **115**, 173907 (2014).

[42] E. Stern-Taulats, A. Gràcia-Condal, A. Planes, P. Lloveras, M. Barrio, J.-L. Tamarit, S. Pramanick, S. Majumdar, and L. Mañosa, Appl. Phys. Lett. **107**, 152409 (2015).

[43] P. Devi, M. Ghorbani Zavareh, C. S. Mejía, K. Hofmann, B. Albert, C. Felser, M. Nicklas, and S. Singh, Phys. Rev. Mater. **2**, 122401(R) (2018).

[44] V. Srivastava, X. Chen, and R. D. James, Appl. Phys. Lett. **97**, 014101 (2010).

[45] Q. Zeng, J. Shen, H. Zhang, J. Chen, B. Ding, X. Xi, E. Liu, W. Wang, and G. Wu, J. Phys.: Condens. Matter **31**, 425401 (2019).

[46] S. Singh, P. Kushwaha, F. Scheibel, H.-P. Liermann, S. R. Barman, M. Acet, C. Felser, and D. Pandey, Phys. Rev. B **92**, 020105(R) (2015).

[47] K. Dubey, P. Devi, A. K. Singh, and S. Singh, J. Magn. Magn. Mater. **507**, 166818 (2020).

[48] R. James and K. Hane, Acta Mater. **48**, 197 (2000).

[49] K. F. Hane and T. W. Shield, Philosophical Magazine A **78**, 1215 (1998).

[50] T. Gottschall, E. Stern-Taulats, L. Mañosa, A. Planes, K. P. Skokov, and O. Gutfleisch, Appl. Phys. Lett. **110**, 223904 (2017).

[51] A. Diestel, R. Niemann, B. Schleicher, K. Nielsch, and S. Fähler, Energy Technology **6**, 1463 (2018).

[52] T. Gottschall, K. P. Skokov, B. Frincu, and O. Gutfleisch, Appl. Phys. Lett. **106**, 021901 (2015).

[53] L. Caron, Z. Ou, T. Nguyen, D. Cam Thanh, O. Tegus, and E. Brück, J. Magn. Magn. Mater. **321**, 3559 (2009), current Perspectives: Magnetocaloric Materials.

[54] S. Ghosh, S. Samanta, J. Sinha, and K. Mandal, Appl. Phys. Lett. **119**, 183901 (2021).

[55] J. Liu, N. Scheerbaum, J. Lyubina, and O. Gutfleisch, Appl. Phys. Lett. **93**, 102512 (2008).

[56] K. Xu, Z. Li, Y.-L. Zhang, and C. Jing, Phys. Lett. A **379**, 3149 (2015).

[57] G. J. Liu, J. R. Sun, J. Shen, B. Gao, H. W. Zhang, F. X. Hu, and B. G. Shen, Appl. Phys. Lett. **90**, 032507 (2007).

[58] P. J. Shamberger and F. S. Ohuchi, Phys. Rev. B **79**, 144407 (2009).

[59] S. Y. Dan'kov, A. M. Tishin, V. K. Pecharsky, and K. A. Gschneidner, Phys. Rev. B **57**, 3478 (1998).

[60] L. Huang, D. Y. Cong, L. Ma, Z. H. Nie, Z. L. Wang, H. L. Suo, Y. Ren, and Y. D. Wang, Appl. Phys. Lett. **108**, 032405 (2016).

[61] J. Liu, X. You, B. Huang, I. Batashev, M. Maschek, Y. Gong, X. Miao, F. Xu, N. van Dijk, and E. Brück, Phys. Rev. Mater. **3**, 084409 (2019).

[62] B. Emre, S. Yüce, E. Stern-Taulats, A. Planes, S. Fabbrici, F. Albertini, and L. Mañosa, J. Appl. Phys. **113**, 213905 (2013).

[63] A. Tekgül, M. Acet, F. Scheibel, M. Farle, and N. Ünal, Acta Mater. **124**, 93 (2017).

[64] Y. Qu, D. Cong, S. Li, W. Gui, Z. Nie, M. Zhang, Y. Ren, and Y. Wang, Acta Mater. **151**, 41 (2018).

[65] M. D. Wilding and E. W. Lee, Proceedings of the Physical Society **85**, 955 (1965).

[66] S. Chatterjee, S. Giri, S. Majumdar, and S. K. De, J. Phys. D **42**, 065001 (2009).

[67] L. Chen, F. X. Hu, J. Wang, J. Shen, J. Zhang, J. R. Sun, B. G. Shen, J. H. Yin, and L. Q. Pan, J. Appl. Phys. **107**, 09A940 (2010).

[68] M. Khan, I. Dubenko, S. Stadler, J. Jung, S. S. Stoyko, A. Mar, A. Quetz, T. Samanta, N. Ali, and K. H. Chow, Appl. Phys. Lett. **102**, 112402 (2013).

[69] S. Samanta, S. Ghosh, S. Chatterjee, and K. Mandal, J. Alloys Compd. **910**, 164929 (2022).